Journal of Applied Mathematics and Physics, 2026, 14(1), 513-522
https://www.scirp.org/journal/jamp
ISSN Online: 2327-4379
ISSN Print: 2327-4352

Research on Space Spectral Imaging System Technology Based on Grating Primary Mirror

Jingjing Ge[1], Guoxian Zheng[1], Yanli Liu[1], Jie Liu[2], Zhiwei Zhao[2], Wen Jiang[2]

[1]Beijing Institute of Space Mechanics & Electricity, Beijing, China
[2]China Academy of Space Technology, Beijing, China
Email: 18210968826@163.com

How to cite this paper: Ge, J.J., Zheng, G.X., Liu, Y.L., Liu, J., Zhao, Z.W. and Jiang, W. (2026) Research on Space Spectral Imaging System Technology Based on Grating Primary Mirror. *Journal of Applied Mathematics and Physics*, **14**, 513-522.
https://doi.org/10.4236/jamp.2026.141027

Received: May 15, 2025
Accepted: January 27, 2026
Published: January 30, 2026

Abstract

In order to improve the space emergency rescue capability at night, a new electro-optical remote sensing with computational imaging under low light conditions is designed. The hyperspectral remote sensing snapshot imaging technology was studied under the conditions of low illumination at night with the spectral resolution 5 nm. We use a long thin grating primary mirror with an optical aperture of rectangle to collect energy. The grating primary mirror can be folded in one direction during emission and unfolded in orbit. Spectral dispersion adopts snapshot spectral imaging, which uses the coding plate to encode in the primary image position, and divides the spectral data cube into 2D space for imaging for improving the system's light energy utilization rate. At the same time, a large-dynamic range ultra-low noise ultra-high gain SPAD device is used for low-light level detection, then the target under the condition of extremely low image signal-to-noise ratio is identified stably. In order to enhance the recognition ability under low SNR 12 dB, the system adopts semantic recognition mode. We set up an experimental spectrograph and the experimental results are compared with predictions from theory. The hyperspectral computational imaging technology was studied under the conditions of low signal-to-noise ratio.

Keywords

Grating Primary Mirror, Computational Spectrum, Aerospace Remote Sensing, Environmental Protection

1. Introduction

At present, the water environment situation in China is as follows: Firstly, water pollution remains relatively severe. In key river basins, the intensity and load of

pollution emissions are high, and the emissions of major pollutants far exceed the environmental capacity of the receiving water bodies. Secondly, potential environmental problems are constantly emerging. Organic pollution has not been eliminated, and long-term accumulated problems such as heavy metals and persistent organic pollutants are beginning to surface. Thirdly, the pressure for pollution reduction continues to increase. Fourthly, environmental risks still exist. The water quality of some centralized drinking water sources is difficult to stably meet the standards, posing potential safety hazards.

Low-light spectral imaging utilizes the natural spectra (visible and near-infrared spectral bands) at night to provide more detailed spectral information [1]-[3]. Hyperspectral technology, by taking advantage of the uniqueness of the target spectrum, has played an important role in environmental monitoring [1] [3]. Low-light hyperspectral imaging makes use of the visible and near-infrared imaging spectral bands [2] [4]. Through the technical approach of low-light spectral imaging, it can enhance the imaging energy, meet the detection requirements under low-illumination conditions such as at dawn, dusk or at night, and can be used alternately with the visible light channel. Since the imaging spectral band is similar to that of the visible light channel, the visual effect of the low-light image is better than that of the infrared image, and a higher spatial resolution can be achieved, which makes up for the problem of insufficient spatial resolution in night imaging detection [3] [5] [6] [7].

However, during traditional night spectral imaging, it is necessary to increase the aperture of the imaging system. But due to the limitations of factors such as the preparation of optical system materials, processing technology, and launch vehicle capacity, the traditional imaging method cannot meet the subsequent needs of aerospace for large-aperture and ultra-large-aperture optical imaging spectrometers. Restricted by factors such as the materials of the optical system, processing costs, and launch vehicle capacity, the implementation cost increases rapidly, and in some cases, it may not even be achievable at all.

2. Method

Since the optical payload is used to obtain hyperspectral data under low-light conditions, the imaging signal-to-noise ratio of the system has become an important issue faced in the development of the optical payload. The following presents the signal-to-noise ratio formula of the system, as shown below:

$$SNR = Signal/(Signal + Noise_{sensor}^2 + Noise_{circuit}^2 + Noise_{other}^2)^{1/2} \quad (1)$$

among them,

$$Signal = flux * t * QE * \lambda_{center}/hc \quad (2)$$

$$Flux = A_{sensor} * \pi * (1 - \varepsilon) * L * T * R_{spectrum}/(4 * F\#^2) \quad (3)$$

$$GSD/H = A_{sensor}/f \quad (4)$$

Thus, it can be concluded that:

$$Signal = GSD^2 * D^2 * \pi * (1 - \varepsilon) * L * T * R_{spectrum} * t * QE * \lambda_{center}/(hc * 4 * F\#^2) \quad (5)$$

Among them, GSD is the spatial resolution, T is the scanning period, L is the radiance, and h is the Planck constant $h = 6.63 \times 10^{-34}\,\mathrm{J \cdot s}$, The speed of light is denoted as $c = 3 \times 10^{8}\,\mathrm{m/s}$. D is the diameter of the optical aperture, ε is the percentage of the optical aperture that is occluded, QE is the quantum efficiency, F# is the F-number of the optical system, T is the transmittance of the optical system, λ_{center} is the central detection of wavelength, $R_{spectrum}$ is the spectral resolution.

From the above expanded formula, it can be known that the positive proportional relationships between the signal-to-noise ratio and the ground resolution (GSD), spectral resolution ($R_{spectrum}$), and radiance (L) are as follows:

$$GSD^2 * D^2 * L * R_{spectrum} \propto SNR \tag{6}$$

From this, it can be seen that under the same system, in order to achieve high-resolution and high-spectral performance, it is necessary to simultaneously improve the spatial resolution, spectral resolution, and reduce the radiance. As the spectral resolution is improved, it will inevitably lead to a decrease in the signal-to-noise ratio of the image. If the signal-to-noise ratio of the image is to be guaranteed, it is necessary to significantly increase the optical aperture (D) of the system.

According to the calculation method of spectral imaging of aerospace remote sensors, under the condition of a full moon night in a 500-kilometer orbit, to achieve a observation with a resolution of 4m/20nm, the aperture of the system needs to be at least Φ10 m (pixel size 28 um, F# 0.3). Firstly, for the weight of a large-aperture optical imaging remote sensing system, the weight of the main mirror of the optical system accounts for the majority. Usually, the weight of the main mirror of the optical system considered only includes the weight of the mirror surface, without reflecting the weight of the support structure. However, the support structure and the active control mechanism also account for a large part of the weight. Internationally, the optical telescope assembly (OTA) is usually used to describe the weight of the main mirror. The surface density of a single sub-mirror of the main mirror in the James Webb Telescope is 15 kg/m^2. However, the surface density of the OTA increases by 5 times after including the support structure, reaching 74 kg/m^2. For the main mirror of a traditional optical system with a diameter exceeding 3 m, the relationship between the surface density and the diameter can be expressed as:

$$\text{Surface density} \propto \text{Aperture diameter}^{2.2} \tag{7}$$

According to the direct proportional relationship formula, for a traditional reflective optical telescope with a Φ10 m aperture, it can be calculated that the surface density is approximately 237 kg/m^2, and its weight will reach 18,605 kg. Secondly, when designing the optical system, it is quite difficult to correct the aberrations of a small F# system like 0.3. In addition, the small depth of focus of the system leads to extremely strict tolerances, making it difficult to ensure the realization of the payload in engineering.

To this end, a new spectral imaging system based on a grating primary mirror is proposed. A new type of ultra-light grating film is used as the primary mirror.

Through satellite push-broom scanning, high-precision detection of spectral information and imaging information of the same ground object information can be achieved over a large range, and at the same time, accurate detection with a large field of view, high spectral resolution, and high spatial resolution can be realized. By using a focal plane array detector (such as iCCD, sCMOS devices, etc.), the scenery within the field of view can be spectrally separated and imaged simultaneously at one time.

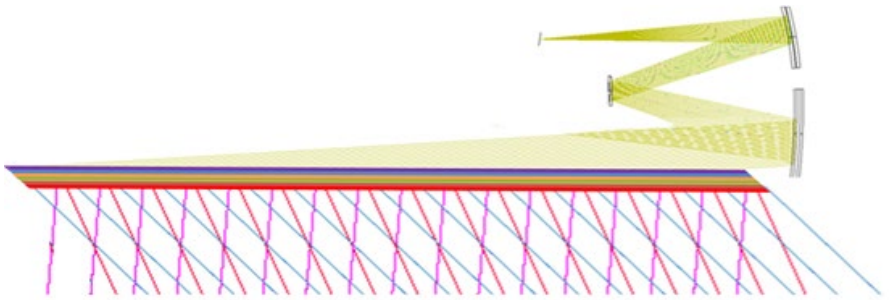

Figure 1. Schematic diagram of the spectral imaging system scheme using a grating primary mirror.

The principle of the imaging technology of the grating primary mirror is shown in **Figure 1**. The collimated light beams with different field angles represent the targets in different angular orientations. At this time, all the spectral information of the target is included. When the light beams are incident on the thin-film planar transmission grating, they are dispersed and split. At a specific and identical diffraction exit angle, the exit light beam corresponding to each field angle only contains the light energy of a specific wavelength. Subsequently, after passing through the optical focusing imaging system, a slit is placed at the primary imaging plane. At this moment, the light energy contained in the slit is the superposition of the light energy of the respective specific wavelengths corresponding to each field angle. By placing a dispersive device again behind the slit and conducting spectral detection, the intensity information of specific wavelengths in different fields of view can be obtained. Through the scanning motion of the system, the light energy distribution of all wavelengths in all field angles can be reconstructed, that is, spectral imaging detection is achieved.

At the same time, the thin-film grating spectral reflector has the advantage of being easy to fold and deploy. By folding the thin-film grating reflector, the entire device can save more space during launch. This design well meets the requirements of ultra-light weight and ultra-large aperture for space reflectors. Different from the traditional reflective primary mirror with a hard substrate, the thin-film grating spectral imaging technology uses a thin-film planar grating device as the primary mirror of the spectral imaging system, which can reduce the surface density of the optical primary mirror by approximately one order of magnitude. It is one of the strong contenders for the technical route of the optical primary mirror of the next-generation space payload. Meanwhile, the length direction of the long-

strip planar grating is utilized to increase the ground energy information, and different diffraction orders of grating diffraction are adopted to compress the optical path, so as to achieve accurate detection with high spectral resolution and high spatial resolution (**Figure 2**).

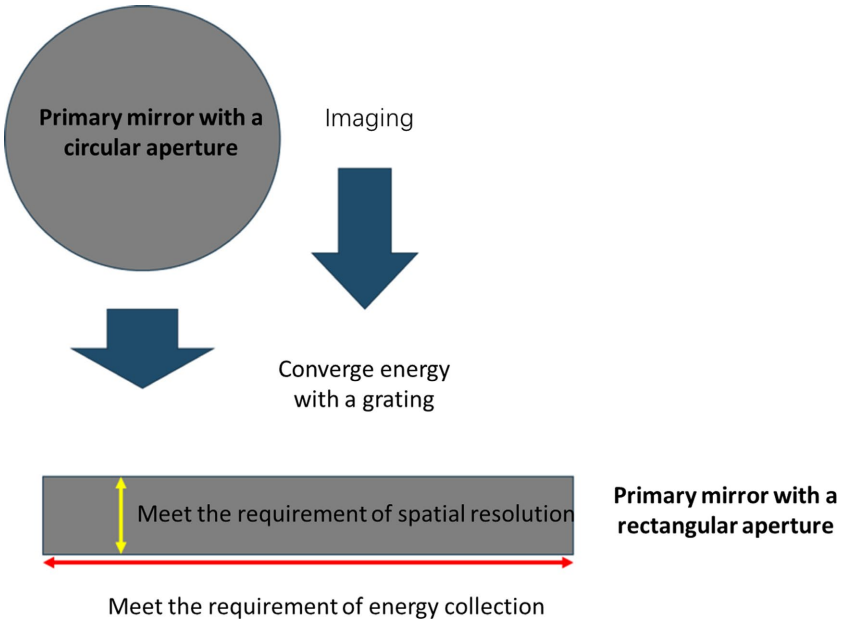

Figure 2. Schematic diagram of the circular aperture and the rectangular long-strip grating

The thin-film grating spectral imaging spectrometer effectively takes advantage of the above-mentioned merits of the spectral imaging technology of the diffraction grating. It accomplishes both dispersion and imaging simultaneously, and is a unique spectrometer with axial dispersion. By combining high spatial resolution and high spectral resolution, it has the advantages of a compact structure, high throughput, and staring imaging with a large field of view.

A desktop system has been designed. A transmissive diffraction planar grating with 1740 lines/mm is adopted. The focal length of the system is 40 mm, the field of view is 18.7˚ × 1˚, and the F-number is 1.2. Among them, the spectral splitting system adopts the design of an image-side telecentric optical path, and the Zemax optical design software is used for design and simulation. The specific design diagram is as follows (**Figure 3, Figure 4**).

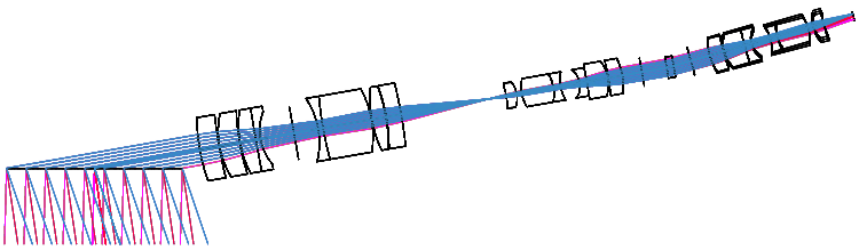

Figure 3. Design and simulation diagram of the imaging spectrometer with a transmissive grating primary mirror.

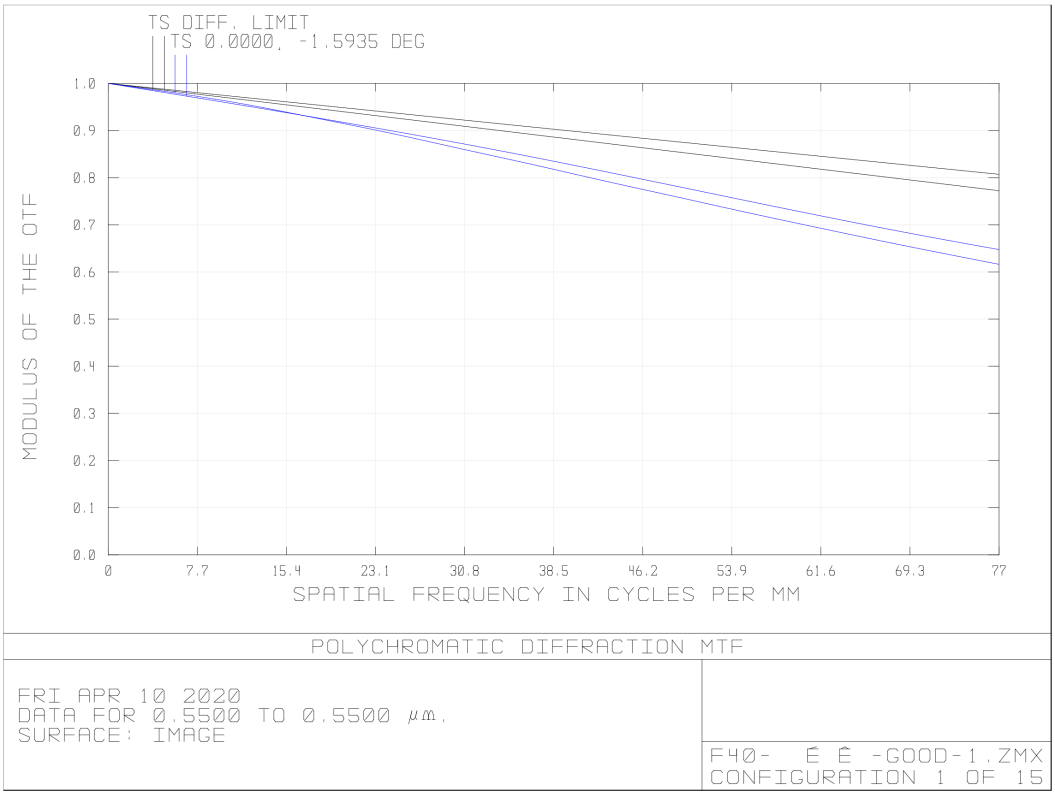

(a)

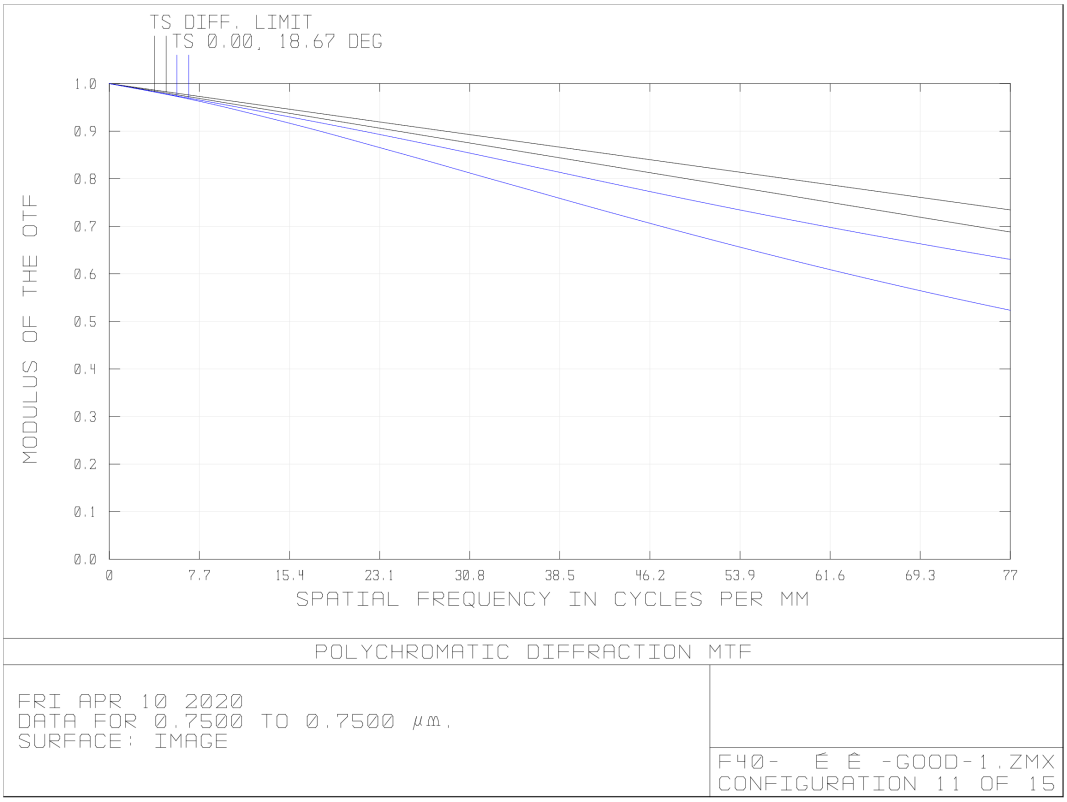

(b)

Figure 4. MTF curve of the imaging system based on the transmissive grating primary mirror.

3. Experiment

According to the results of the optical simulation verification, a desktop verification device was built, and the experimental device is shown as follows (**Figure 5**).

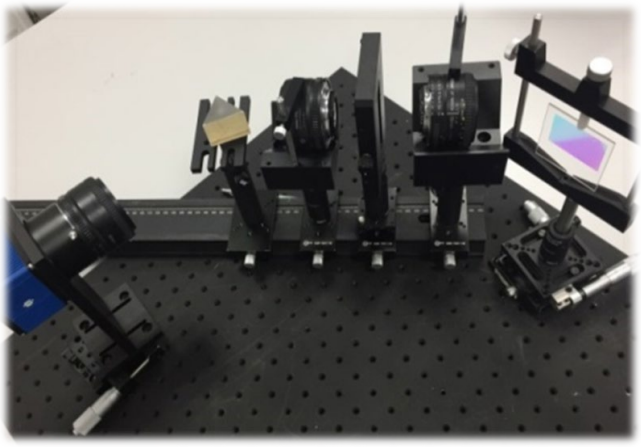

Figure 5. Schematic diagram of the desktop principle experimental device.

The 0^{th}-order image of the grating and the 1^{st}-order spectral image collected at the detector end are shown on the left side of the following **Figure 6**, and the color effect is shown on the right side of the **Figure 6**.

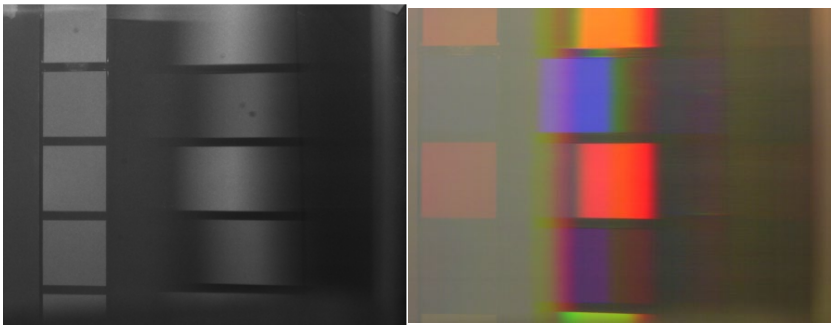

Figure 6. Imaging results of the system (the grayscale image is on the left and the color image is on the right)

After extracting the spectrum, a dispersed single-spectrum image at the position of the primary image is obtained. The spectra of some spectral bands are shown in the following **Figure 7**.

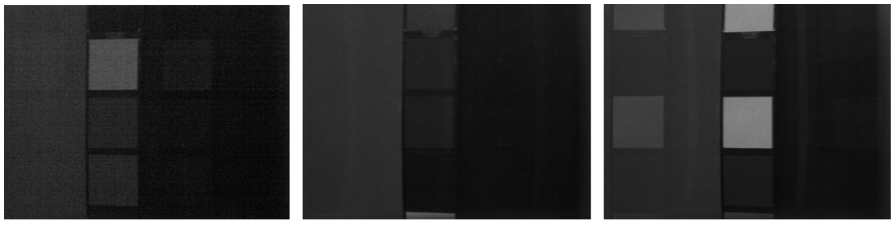

(432nm) (532nm) (632nm)

Figure 7. Single-spectrum image at the position of the primary image.

The dispersed single-spectrum image at the position of the primary image is subjected to spectral translation correction, and the spectral images of all spectral bands are shown in the following **Figure 8**. The spectral resolution reaches 5 nm.

The spectra of some spectral bands are shown in the following **Figure 8** which

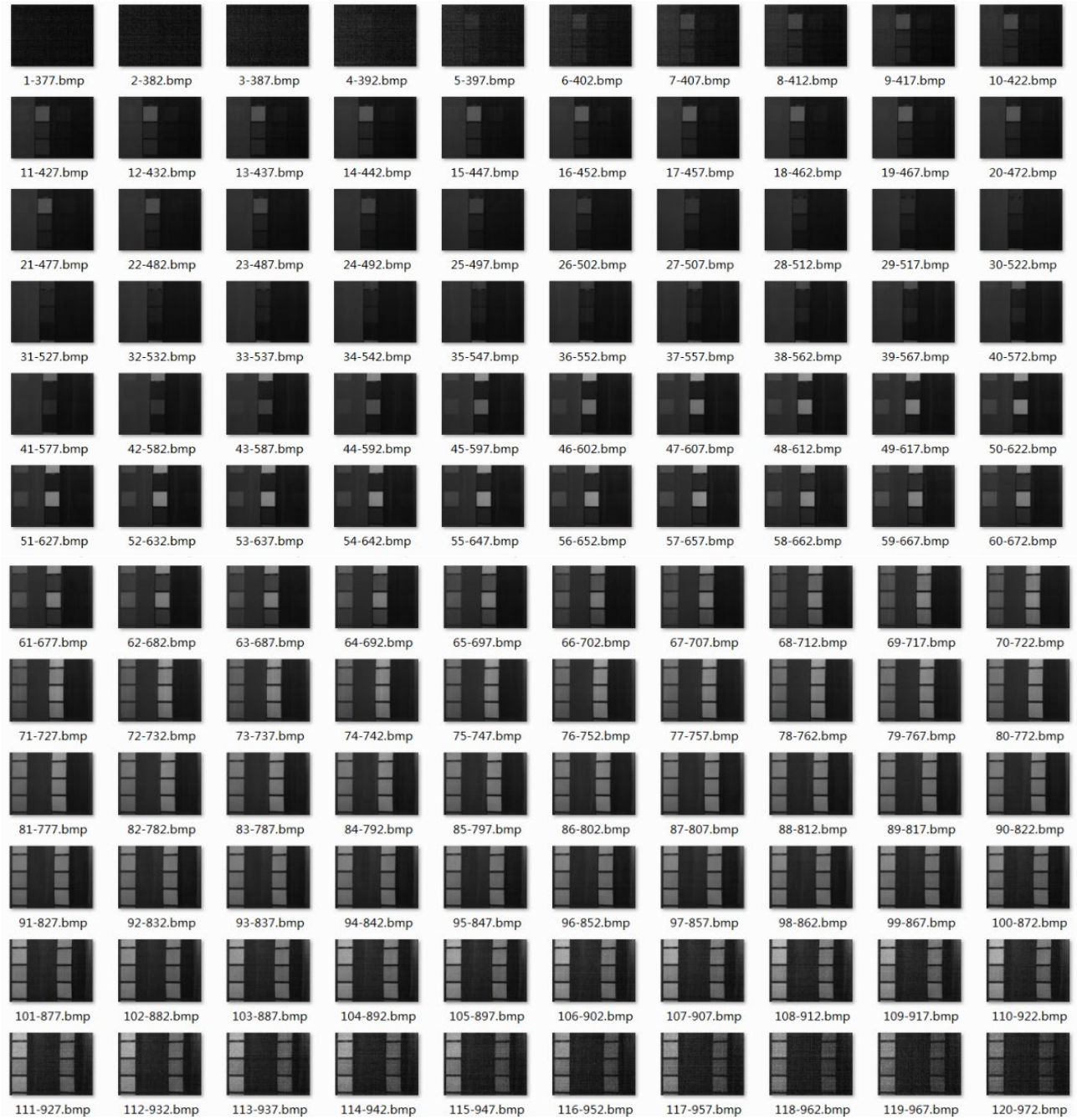

Figure 8. Spectral images of each spectral band.

select the red, green and blue spectral bands (433 nm, 518 nm, 620 nm) for color synthesis to obtain the target color image as shown on the left of the following **Figure 9**. The image on the right is the original color image of the target. The color

synthesis effect of the spectrum is highly consistent with the original color of the target (**Figure 10)**.

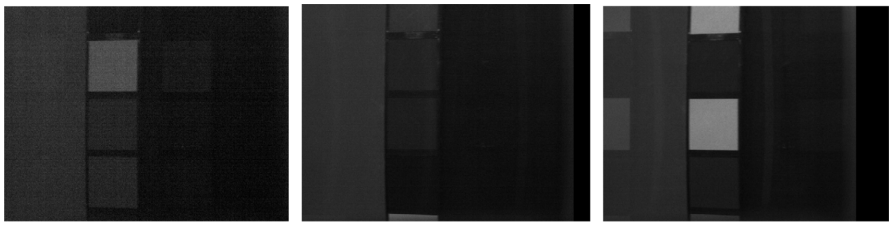

(432nm) (532nm) (632nm)

Figure 9. Single spectral band image.

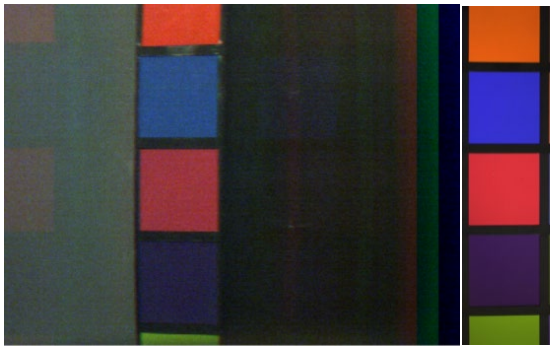

Figure 10. Color composite image of the target (left image) (right image: original color image of the target).

4. Conclusion

To enhance the spectral imaging capability at night, we propose a new imaging method: the space-based spectral imaging system technology based on a grating primary mirror. This method collects energy through a long-strip grating primary mirror and acquires the target image using computational spectral imaging. The results of the imaging experiment show that the principle of the slit push-broom imaging technology based on the reverse grating primary mirror is feasible, and it can achieve spectral imaging with high spatial resolution and high spectral resolution in the visible and near-infrared spectral bands, with a spectral resolution of 5 nm.

Acknowledgements

This research was supported by the National Natural Science Foundation of China (U234120347).

Conflicts of Interest

The authors declare no conflicts of interest regarding the publication of this paper.

References

[1] Lee, T.E., Miller, S.D., Turk, F.J., Schueler, C., Julian, R., Deyo, S., *et al.* (2006) The

NPOESS VIIRS Day/Night Visible Sensor. *Bulletin of the American Meteorological Society*, **87**, 191-200. https://doi.org/10.1175/bams-87-2-191

[2] Li, X. and Li, D. (2014) Can Night-Time Light Images Play a Role in Evaluating the Syrian Crisis? *International Journal of Remote Sensing*, **35**, 6648-6661. https://doi.org/10.1080/01431161.2014.971469

[3] Elvidge, C., Zhizhin, M., Baugh, K. and Hsu, F. (2015) Automatic Boat Identification System for VIIRS Low Light Imaging Data. *Remote Sensing*, **7**, 3020-3036. https://doi.org/10.3390/rs70303020

[4] (2016) DMSP-Block 5D-3 Spacecraft Overview. http://www.astronautix.com/d/dmspblock5d-3.html

[5] Visible Infrared Imaging Radiometer Suite (VIIRS). https://ncc.nesdis.noaa.gov/VIIRS/

[6] Elvidge, C.D., Cinzano, P., Pettit, D.R., Arvesen, J., Sutton, P., Small, C., *et al.* (2007) The Nightsat Mission Concept. *International Journal of Remote Sensing*, **28**, 2645-2670. https://doi.org/10.1080/01431160600981525

[7] Zhang, Q. and Seto, K. (2013) Can Night-Time Light Data Identify Typologies of Urbanization? A Global Assessment of Successes and Failures. *Remote Sensing*, **5**, 3476-3494. https://doi.org/10.3390/rs5073476